



FINAL PUBLISHABLE JRP REPORT

JRP-Contract number	SIB03	
JRP short name	KNOW	
JRP full title	Realisation of the awaited definition of the kilogram – resolving the discrepancies	
Version numbers of latest contracted Annex Ia and Annex Ib against which the assessment will be made	Annex Ia:	V1.1
	Annex Ib:	V1.1
Period covered (dates)	From	01 September 2012 To 31 August 2015
JRP-Coordinator		
Name, title, organisation	Giovanni Mana, Dr, INRIM	
Tel:	+39 0113919728	
Email:	g.mana@inrim.it	
JRP website address	http://www.inrim.it/luc/know/index.php	
Other JRP-Partners		
Short name, country	CNAM, France; METAS, Switzerland; LNE, France; OBSPARIS, France; PTB, Germany; AIST, Japan; IOM, Germany	
REG-Researcher		
Researcher name, title	Fred Pietag, Dr	Start date: 01/09/2012
Home organisation	IOM, Germany	Duration: 36 months
Researcher name, title	Hendrik Paetzel, Dr	Start date: 01/01/2013
Home organisation	IOM, Germany	Duration: 18 months
Researcher name, title	Luciano Colombo, Prof.	Start date: 01/11/2013
Home organisation	Cagliari University, Italy	Duration: 12 months

Report Status: PU Public



TABLE OF CONTENTS

1	Executive Summary	3
2	Project context, rationale and objectives	4
2.1	Counting atoms	5
2.2	Watt balance experiment.....	6
2.3	Research results	8
2.4	Measurement of the Planck constant	9
2.4.1	Watt-balance experiment: LNE	9
2.4.2	Watt balance experiment: METAS	11
2.5	Measurement of the Avogadro constant.....	15
2.5.1	Molar mass.....	15
2.5.2	Lattice parameter	16
2.5.3	Sphere manufacturing and surface characterization	17
2.5.4	Sphere volume.....	19
2.5.5	Sphere mass	19
2.5.6	Determination of the Avogadro constant	20
2.6	Solving the discrepancies.....	20
2.6.1	Speed of light effect in free-fall gravimeters	20
2.6.2	Coil-magnet interaction: continuous model.....	20
2.6.3	Coil-magnet interaction: electrostatic forces.....	21
2.6.4	Stress and strain of Si surface	21
2.6.5	Nuclear activation determination of the ³⁰Si fraction	21
2.6.6	Elemental analysis of the ²⁸Si purity by nuclear activation	21
2.6.7	Consistency of the Planck constant values	22
2.6.8	Correlation of the N_A measurements	22
2.7	Key results	22
3	Actual and potential impact	23
4	Website address and contact details	25
5	Participants and collaborators	25
6	List of acronyms	26
7	List of publications.....	26

1 Executive Summary

In 2018 the kilogram definition will change. One kilogram will be defined in terms of the Planck's constant, rather than by using a physical object, to ensure the definition can support future scientific and industrial innovation. This requires independent accurate determinations of Planck's and Avogadro's constants. In 2011 two methods were used to calculate Planck's constant, but results were inconsistent and not sufficiently accurate for the redefinition. This project refined and improved the two approaches, to increase the accuracy to which they can state Planck's constant, to ensure their results are consistent, and, ultimately, to ensure they can be used for the redefinition

The Problem

Today, the kilogram, the SI base unit of mass, is defined as the mass of the International Prototype Kilogram (IPK), a platinum-iridium cylinder kept in a vault of the Bureau International des Poids et Mesures in Paris. This definition is not capable of supporting future increases in definition accuracy, of ensuring long-term stability, and it is not sufficiently accessible. Although copies have been distributed globally, access to the IPK is limited to rare verifications; since 1889, only four. In addition, the masses of the IPK and of its copies fluctuate over time as atoms are lost and/or adhere to their surfaces. Eventually, all today precision measurements that requires traceability to the kilogram lack a firm and stable anchor to fundamental properties and/or constants of Nature, an essential requirement to ensure long-term significance of the results.

Solution

In 2011 it was decided the kilogram would be redefined in terms of Planck's constant, a naturally occurring quantity whose value can set upon international agreement to constrain the unit of mass. The Planck's constant is a measurement of the quanta of a physical quantity named action; ultimately, it can be related to mass and frequency by Einstein's and Planck's equations $E = mc^2$ and $E = h\nu$. Formally, $m = h\nu/c^2$, where ν is a suitable frequency. Therefore, such a definition would be accessible through experimentation and would support future refinements in accuracy and a standard laboratory method is needed to determine h given m , which will be used in reverse to determine m given h . Two independent experiments are under consideration, a watt-balance method (which determine h from the IPK mass) and an atom-counting method (which determine h from its ratio to the Si 28 mass).

Impact

The project made a major contribution to the kilogram redefinition including:

- Demonstrated that counting silicon atoms to within the needed accuracy is possible;
- Delivered an additional extremely accurate value of the Avogadro constant – $N_A = 6.02214076(12) \times 10^{23} \text{ mol}^{-1}$, having an uncertainty of 20 atoms per billion – in order to fix the best possible value of the Planck constant;
- Developed a European approach to the watt-balance technologies;
- Delivered a watt-balance determination of the Planck constant – $h = 6.6260688(20) \times 10^{-34} \text{ J s}$ – that, though not yet reaching a competitive accuracy, is consistent with the measured N_A value.

In the meantime the overseas competitors (NIST, in USA, and NRC, in Canada) carried out similar stress-tests on their watt-balance experiments and repetitions of the h measurement. The NIST result, though not yet competitive, is consistent with the atom-counting N_A value, while an excellent agreement has been reached between the project and NRC experiments.

The kilogram redefinition will make precision measurements more readily available. However, few labs can cover the cost of a primary realisation based on the watt balance or atom counting technologies. Therefore, future work will aim at maintaining and disseminating the kilogram via monocrystalline natural silicon spheres, whose initial calibration is kept alive by surface characterisation and volume measurements. This would require the development of appropriate methods for a cheap manufacture of high accuracy monocrystalline silicon spheres and the geometrical, physical, and chemical characterization of their surface. This will also help to disseminate the kilogram to industry with a high accuracy and reasonable costs.

2 Project context, rationale and objectives

Mass metrology relies on a traceability chain ending in the International Prototype of the kilogram (IPK), which is nearly permanently stored in a vault of the Bureau International des Poids et Mesures (BIPM). The obvious reason is that the accumulation of surface contaminants and wear might lead to irreversible mass variations. Consequently, since the IPK was sanctioned by the 1st Conférence Générale des Poids et Mesures in 1889, only four verifications were made, in 1889, 1946, 1991, and 2014. The mass of the national copies was observed to drift, on the average, by 50 μg in a century. Figure 1 shows the mass drift of the official BIPM copies. In practice, the traceability chain ends in BIPM's working standards that were calibrated against the IPK on the occasion of the few verifications, but these working standards have been shown to loose mass with the usage.

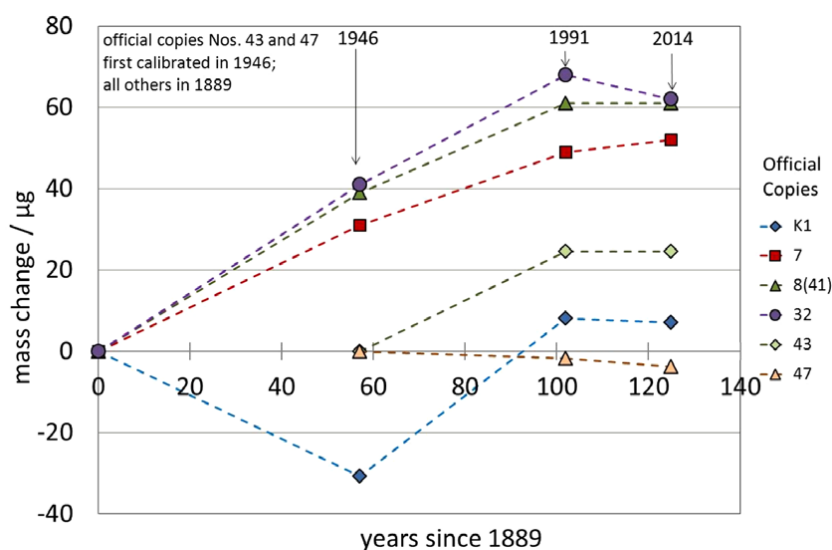


Figure 1. Evolution in mass since the first calibration of the official copies. Official copies nos. 43 and 47 were first calibrated in 1946, all others in 1889. The standard Type A uncertainties of each of these data points are: 3.2 μg (1889); 5.4 μg (1946); 2.3 μg (1991); about 1 μg (2014). All masses are shown as deviations from 1 kg (M Stock *et al.* *Metrologia* **52** 2015 310).

Other units previously defined by an artefact were redefined in terms of fundamental constants of physics. The classical example is the metre, which is defined as the distance travelled by light in $1/299792458$ s. Another example is the ampere, which relies on the conventional $4\pi \times 10^{-7}$ N A⁻² value of the magnetic constant. The artefact-based definition of the kilogram is exposed to instability: the mass of the national copies is known to drift, on the average, by 50 μg in a century. This means that they must be periodically sent to the BIPM for calibration. Additionally, the prototype stability might not be much better than that of its copies. To overcome the difficulties of mass metrology, it has been proposed that the kilogram is redefined by fixing a conventional value of the Planck constant, but it is necessary to demonstrate that the new realizations do not differ from the IPK more than 20 μg .

The energy E of a quantum system is linked to the frequency ν of its quantum-mechanics wave function by the Planck equation $E = h\nu$. Consequently, in quantum physics, the Planck constant h converts energy units into frequency units and vice versa. Additionally, when quantum mechanics is combined with relativity, the Planck constant also links the Compton frequency ν_C of a relativistic wave (in the reference frame where the system is at rest) to its mass-energy $E = mc^2$. By combining the Planck and Einstein equations, we obtain $h\nu = mc^2$, which identify frequency and mass and shows that h/c^2 is the conversion factor between frequency and mass units.

In practice, since the second definition fixes the frequency ν_{Cs} of the photon emitted in the transition between two quantum states of the cesium 133 atom, by fixing – in addition to the speed of light – the Planck constant, the difference between the masses of the ¹³³Cs atom in the excited and ground states is exactly $h\nu_{Cs}/c^2$ by definition. Therefore, this mass difference would replace the current Pt-Ir prototype as a standard of mass. The

next problem to be addressed by improved measurement capabilities is to scale up this extremely tiny mass, about 7×10^{-38} g, to a macroscopic value, to within a relative uncertainty better than 2×10^{-8} .

Two ways, counting the atoms in a silicon crystal and comparing mechanical and electrical forces or powers via watt balances, demonstrated the potential to perform this task and will be presently illustrated. Consequently, the project objectives were: i) to demonstrate that silicon atoms can be counted to within the needed accuracy; ii) to deliver a value of the Avogadro constant accurate enough to fix the best possible value of the Planck constant; iii) to develop an European approach to the watt-balance realization; iv) to solve the discrepancy between the 2011 measured-values of the Avogadro and Planck constants.

2.1 Counting atoms

The atomic theory of matter and additivity provide the framework to base mass metrology on atom masses. If an atom is chosen as mass standard, say, the silicon 28 one, mass measurements are traced back by counting atoms. A number of experiments measured the h/m_e , h/m_n , $h/m(^{133}\text{Cs})$, and $h/m(^{87}\text{Rb})$ ratios via the Planck and de Broglie equations. Since, as regards atoms and sub-atomic particles, molar masses are well known, these experiments deliver accurate values of the $h/m(^n\text{Si})$, where ^nSi is any silicon isotope.

To convey a macroscopic count into practice, enriched ^{28}Si crystals are shaped as quasi-perfect spheres; the atom number is obtained from volume, V , and lattice parameter, a , measurements. In a formula, $N(\text{Si}) = 8V/a^3$, where $a^3/8$ is the atom volume and 8 is the number of atoms in the cubic unit cell. The count uses silicon crystals because, owing to the demands of modern electronics, they can be grown as high-purity, large, and quasi-perfect single crystals.



Figure 2. A kilogram realization by means of a silicon crystal of spherical shape. An x-ray interferometer used to measure the volume of Si atom in the crystal is mirroring in the sphere (courtesy of E Massa and C P Sasso).

The crystals are never isotopically pure. Therefore, the amount of substance fraction of the Si isotopes and, then, the mean atomic mass, is measured by absolute mass-spectrometry. The need of enriched ^{28}Si crystals stems from the present incapacity to determine the amount of substance fraction of the Si isotopes in natural silicon to within the needed accuracy. Crystals may contain impurities, interstitial atoms, and vacancies, which implies that the counted lattice nodes do not correspond to the number of silicon atoms. This means that crystals must be characterized both structurally and chemically, so that the appropriate corrections are applied. The mass, thickness and chemical composition of the oxide layer covering the sphere must also be taken into account; they are measured by optical and x-ray spectroscopy and reflectometry.

The formation enthalpy of a silicon crystal (the energy lost by one mole of a dilute gas when it forms a crystal at absolute zero) is about 450 kJ/mol; this means that the binding energy contribution to the crystal mass is 5

ng/mol or 0.2 ng/g, in relative terms. According to the Dulong and Petit law, the molar heat capacity of a crystal is $3R$, where $R = 8.314 \text{ JK}^{-1}\text{mol}^{-1}$ is the gas constant. Therefore, in the case of a silicon crystal at room temperature, the contribution of thermal energy to crystal mass is 75 pg/mol or 3 pg/g, in relative terms.

2.2 Watt balance experiment

A direct way of measuring the h/m ratio, where m is a macroscopic mass, is by a watt balance. This device virtually compares the electrical and mechanical powers required to move a mass with uniform vertical velocity against the Earth gravity. The comparison is carried out in two steps. Firstly, the balance is used to compare the mass weight with the force generated by the interaction between the electrical current in a coil supporting it in a magnetic field. Secondly, the coil is moved with uniform velocity and the induced electromotive force is measured. By combining the relevant measurement equations, the h/m ratio is obtained.

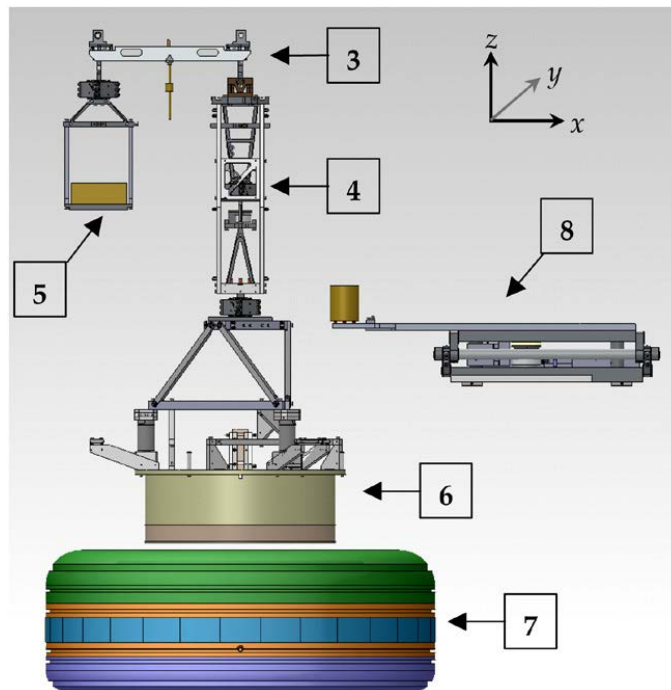


Figure 3. Schematic of the LNE watt balance; balance beam (3), suspensions (4, 5), coil (6), magnetic circuit (7), mass exchanger (8). The translation stage is not shown.

In the static phase, or force measurement, the force generated by a mass m placed in the local gravity field g , is balanced by the vertical component of the electromagnetic force produced by a current I flowing in a coil immersed in a magnetic field B (Fig. 4 left). The electromagnetic force can be expressed by

$$m \cdot g = \vec{F} = I \cdot \oint d\vec{l} \times \vec{B}, \quad (1)$$

where l is the conductor length of the coil. In the dynamic phase, or induction mode, the coil is moved vertically at a velocity v through the magnetic field B (Fig. 4 right). This motion induces a voltage U across the coil that can be expressed by

$$U = -\oint (d\vec{l} \times \vec{B}) \cdot \vec{v}. \quad (2)$$

If the magnetic field and the mechanical dimensions of the coil are identical in both modes, and under the hypothesis that the coil passes through its weighing position during the velocity mode with the same orientation, it can be shown that the combination of both phases leads to a virtual comparison between the mechanical and the electrical power. This can be summarized by

$$U \cdot I = m \cdot g \cdot v. \quad (3)$$

The experiment thus allows a virtual comparison between the electrical and the mechanical power. Using the expressions of the quantum Hall and Josephson effects, equation (3) can be rewritten as

$$m = C \cdot \frac{f_J f'_J}{g \cdot v} \cdot h, \quad (4)$$

where C is a calibration constant, f_j and f_j' are the Josephson frequencies used during the static and the dynamic phase and h the Planck constant. The watt balance experiment allows therefore relating the unit of mass to the meter, the second and the Planck constant.

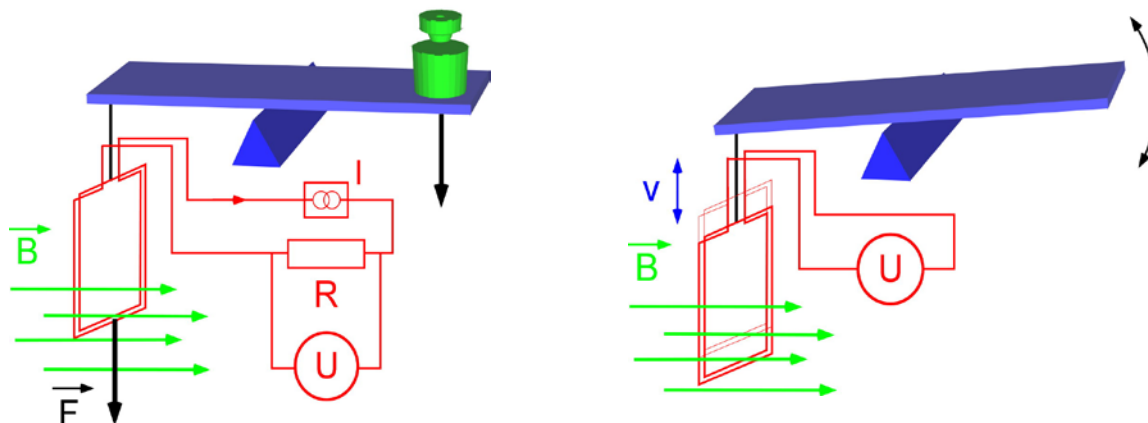


Figure 4. Left: Static mode: The electromagnetic force acting on the current carrying coil is balanced against the weight of the test mass. Right: Dynamic mode: the coil is moved in the vertical direction through the magnetic field and the induced voltage is measured.

2.3 Research results

Objective 1: CNAM, METAS, LNE, and OBSPARIS fine-tuned and adjusted two European watt balances to their maximum performance level

In 2011 the METAS completed a measurement of the Planck constant having a $3 \times 10^{-7}h$ uncertainty, which revealed the ultimate limits of the technologies then developed. The METAS realized a new watt balance, whose critical components were redesigned with the support of the Laboratoire de Systèmes Robotiques of the École Polytechnique Fédérale de Lausanne, CERN, and Mettler-Toledo.

In 2012, the CNAM, LNE, and OBSPARIS operated a watt balance at the $5 \times 10^{-5}h$ accuracy level. The project tuned this balance – by pinpointing and solving the problems – up to reach a $31 \times 10^{-8}h$ accuracy.

Objective 2: CNAM, LNE, and OBSPARIS carried out h measurements with 31×10^{-8} relative uncertainty via a watt-balance experiment

This objective has not been fully reached. The redesign and replacement of the inadequate components, and the testing of the new ones, delayed the balance operation and prevented the measurement of the Planck's constant to the targeted 5×10^{-8} relative uncertainty. The best measurement was completed at LNE in December 2014, with a relative uncertainty of 31×10^{-8} . The LNE carried out an additional measurement campaign in March 2016; the data analysis is under way. The METAS watt balance is operational since May 2016 and investigations to exclude or to quantify systematic errors are under way.

Objective 3: INRIM, NMIJ, PTB, IOM, REG(IOM), and REG(UNICA) challenged all parts of IAC experiment and confirmed the measured N_A value and its uncertainty

The measurement of N_A was improved by pushing all the techniques involved to their limits. PTB re-polished and measured anew the two silicon spheres of the IAC. To estimate the surface effect on the measurements of the spheres, REG(UNICA) carried out density functional calculations of the strain and stress of silicon surfaces. The REG(IOM) the PTB developed ion-beam technologies and interferometers to re-measure the surfaces and the volumes of the spheres. NMIJ and PTB repeated molar mass measurements by substituting tetramethylammonium hydroxide for sodium hydroxide as the silicon solvent and diluent. In addition, INRIM confirmed by nuclear activation the molar fraction of the ^{30}Si isotope. INRIM and ANSTO verified experimentally the material purity with respect to a large number of contaminating elements by nuclear activation analysis. INRIM totally rebuilt the optical interferometer used to measure the silicon lattice parameter, using different optical components and a different wavelength. The project demonstrated that the counting of silicon atoms to the required level of accuracy is possible, and that no error was made in this respect in the 2011 experiment.

Objective 4: INRIM, NMIJ, and PTB repeated the N_A determination by simultaneously reducing the relative uncertainty to 1.5×10^{-8}

This objective was almost achieved, as the refined approach allowed N_A to be measured to within an uncertainty of 20 atoms per billion (2.0×10^{-8}).

Objective 5: the consortium, in collaboration with NIST and NRC, investigated and removed the discrepancy between the watt-balance and atom-counting determinations of h and N_A

The 2011 inconsistencies in the measured values of h and N_A prompted an investigation into a number of effects that could potentially cause systematic errors. For the watt-balance method, research focussed on the effects of: i) the finite speed of light on the operation of the free-fall gravimeters used to determine the local acceleration of gravity; and ii) the interactions between the watt-balance coil and magnet. For the atom-counting method, research focussed on the effects of i) the surface stress and strain on the lattice-parameter and sphere-volume measurements; ii) the contamination of the enriched crystal on the count of the Si atoms; iii) the NaOH dissolving and dilution matrix on the measurement of the abundance of the minority Si isotopes; and iv) the correlation of the N_A measurements. Although a few of these effects approached the experiment sensitivity, none were found to be critical at the desired level of accuracy.

Objective 6: the consortium, in collaboration with BIPM, carried out h and N_A determinations involving comparisons traceable to the international prototype of the kilogram.

The International Bureau of Weights and Measures (BIPM) carried out an extraordinary calibration campaign to ensure the results of the atom-counting and watt-balance experiments could be linked to the IPK.

The BIPM prototypes, the BIPM ensemble of mass standards, and the mass standards used in the h and N_A determinations were compared as directly as possible with the IPK, to reveal any inconsistencies in mass introduced at each key step of each method. The campaign was successful, and an offset of around 35 μg (35 billionths of a kilogram) was identified and corrected for. The creation of methods to define the kilogram external to the IPK means that the watt-balance and atom-counting approaches can also be used to monitor how the mass of the IPK and its copies fluctuates over time.

Objective 7: the consortium, in collaboration with NIST, NRC, and BIPM, demonstrated consistent kilogram realisations based on both the h and N_A determination

In addition to the project's European partner, the project team worked with the wider international metrology community outside Europe. The National Institute of Standards and Technology (NIST) in USA, and the Standards Laboratory of the Canada's National Research Council (NRC) in Canada – carried out similar stress-tests on their watt-balance experiments and repeated their h measurements. The 2014 watt-balance determination of h carried out by NRC was consistent with this project's value of N_A ; and the measurement repetition of h by NIST's watt-balance resulted in an improved agreement with this project's value of h . Results from the two methods, in the three different locations, are converging. Therefore the impediments to a kilogram redefinition by fixing the value of Planck's constant are being removed.

2.4 Measurement of the Planck constant

The need of European autonomous realizations of the kilogram and the 2011 discrepancy between Planck's constant values obtained by the NIST and NRC watt-balance experiments prompted efforts to demonstrate independent measurement results.

2.4.1 Watt-balance experiment: LNE

After separate developments of the different elements with continuous characterizations and improvements, the watt balance was assembled and tested. LNE developed calibration methods for the detectors that monitor the position and attitude of the moving coil. Sub-divisional error, linearity error and dilatation of the calibration device were checked against an interferometer. Calibration of coil sensor position is done with a standard uncertainty below 100 nm.

A measurement of the Planck constant was done in Dec 2014 by a LNE, CNAM and OBSPARIS collaboration. The watt balance was operating in air with a mass of 500 g. The value

$$h = 6.626\,068\,8(20) \times 10^{-34} \text{ Js}$$

has been determined with a relative combined uncertainty of 3.1×10^{-7} . The main uncertainty contributions are summarized in table 1.

Subsequently, parts of the experimental set-up was significantly improved with the aim at reducing the major uncertainty components: a Josephson voltage standard has been integrated in the measurement apparatus; a single-piece beam and a coil suitable for vacuum operation substituted for the balance beam and coil and have been successfully tested; the vacuum system has been implemented and successfully tested; the Pt-Ir test mass has been characterized and it is ready to use. A full-cycle test of the watt balance is in progress and would allow a new campaign of in air h measurements to be started soon.

Table 1. Main uncertainty contributions of the Planck constant determination (LNE, CNAM, and OBSPARIS collaboration).

uncertainty contribution	relative standard uncertainty
Type A	8.0×10^{-8}
Type B	
Voltage measurements	2.4×10^{-7}
Resistance measurement	6.0×10^{-9}
500 g XSH Alacrite mass (traceability to the national prototype of the kilogram, buoyancy, magnetic susceptibility and XSH Alacrite density contributions)	
Absolute gravity value	7.4×10^{-8}
Velocity measurement (air refractive index and verticality of the laser beams)	5.0×10^{-9}
Parasitic watt ratio term	
Force comparator contribution	1.2×10^{-7}
Other contributions (switch effect*, polynomial fitting**, trigger delay, hysteresis of the flexure strips)	9.1×10^{-8}
	3.3×10^{-8}
	5.0×10^{-8}
Combined relative uncertainty	3.1×10^{-7}

* The switch effect term concerns the performance of the commercial Data Proof low thermal scanner used for automating measurements of the static and dynamic phases.

** The 3rd and 4th order polynomial fits have been also tested and the differences obtained compared to the second order are lower than 5×10^{-8} . Moreover, the histogram of the residual of the second order adjustment is Gaussian contrary to the 3rd and 4th. Considering that the relative standard uncertainty associated with h measurements is 3.1×10^{-7} , these differences have been considered, for the moment, as negligible contributions.

The h determination was carried out by using a balance beam, integrated into the apparatus in 2005 and whose mechanical behavior was studied since then. It uses flexure strips made from a 20 μm thick stainless-steel sheet clamped between two jaws at both ends. Although the results obtained were quite satisfactory, it was decided to build a new beam free from the drawbacks of the 2005 one. In particular, it was difficult i) to clamp the strips without stress and to adjust them correctly, ii) to ensure the parallelism and the co-planarity of the axes of rotation, and iii) to determine the radius of curvature of the hinge since it varied with applied load. In 2014, the CNAM designed a new beam with machined copper-beryllium pivots having an elliptical neck of 40 μm thickness. Attaching and adjusting these pivots to the beam was greatly simplified. Moreover, their radius of curvature did not depend on the load. However, although improved, this design did not yet ensure the parallelism and the co-planarity of the axes of rotation. In addition, although the central pivot is twice as wide as the end pivots, sometimes the beam yaws, which leads to an increased settling time.

Consequently, the CNAM designed a monolithic beam made of aluminum alloy and manufactured by wire-cut Electrical Discharge Machining. The three beam-pivots have elliptical necks of 40 μm thickness and were machined so as to guarantee that their axes are parallel and co-planar. The central pivot is formed by two flexure parts, enough spread to reduce yawing. Now, the axes of rotation are co-linear by machining. The mechanical behavior of this monolithic beam was characterized and checked in a test-bench similar to an electro-dynamometer. It was demonstrated that stability and sensitivity have been improved. Subsequently, the monolithic beam was integrated into the watt balance. The first static phase measurements demonstrated an improved Allan variance.

As regards the real-time measurement of the gravity acceleration at the balance proof-mass centre, the OBSPARIS installed at LNE a superconducting gravimeter next to the watt balance laboratory. This instrument measures gravity continuously with a 1 Hz sampling rate. In the last two years, repeated comparisons against the OBSPARIS' cold atom gravimeter were carried out, over time windows ranging from a few days up to 1 month. These comparisons allowed to i) calibrate the superconducting gravimeter to within an accuracy of 0.1%, ii) assess this calibration over two years at the same accuracy level, iii) demonstrate a calibration drift as low as $3.8 \times 10^{-8} \text{ ms}^{-2} \text{ y}^{-1}$, and iv) demonstrate the reading difference between the two instruments is stable

in the $10^{-10}g$ range, for measurement times as long as one month. Continuous gravity measurements are therefore available, with an uncertainty of $5 \times 10^{-9}g$, which results from the inaccuracy of the cold atom gravimeter, $4 \times 10^{-9}g$, combined with the uncertainty of the transfer between the position of the balance proof-mass and the position of the atoms in the gravimeter, $3 \times 10^{-9}g$. The accuracy of the cold atom gravimeter was validated by a comparison of absolute gravimeters carried out in Walferdange, Luxembourg, in 2013.

The LNE carried out an additional measurement campaign in March 2016 (outside of this project); the data analysis is under way.

2.4.2 Watt balance experiment: METAS

The main components of the METAS watt balance are shown in Fig. 5 (left). The driving stage, placed at the top of the experiment, is based on the principle of a Sarrus linkage. It moves the coil through the magnetic field during the dynamic phase of the experiment. The straightness of movement along the vertical trajectory is ensured by the guiding stage formed by a monolithic 13-hinge stage. The whole suspension holding the coil is attached to the mass comparator which is inserted in the driving stage. The behavior of the complete mechanism, composed by the guiding stage, the 13-hinge stage, the mass comparator, the suspension, and the coil was evaluated. The deviation along the verticality is 200 nm in y and 40 nm in x for a total path of 38 mm. The magnetic circuit where the coil is encapsulated can be adjusted in x , y , θ_x and θ_y by means of a double gimbal that contains the magnetic circuit. Finally, the position of the coil is measured with a laser interferometer. The mass pan is placed at the bottom of the suspension. By placing the mass at the lowest place of the suspension, it can be ensured that all components will see the same forces during both steps of the static phase of the experiment. The mass exchanger is used to place the test mass on and off the mass pan.

It is a fundamental requirement that only the magnetic field, responsible for the vertical electromagnetic force in the static phase, produces an induced voltage in the dynamic phase. Special attention has been paid to this high critical point during the conception of the suspension-coil assembly. To minimize the Abbe errors, the main mirror, used for the measurement of the coil position in x , y and z is located at the center of the coil (Fig. 5, right). Three flat mirrors and three corner cubes placed on the top of the coil are used to determine its attitude (Fig. 5, right). In the static phase, to distinguish the lateral forces from the torque acting on the coil, the link between the mass comparator and the coil owns two articulations. The first is located at the output of the mass comparator and the second one in the middle of the central tube of the suspension.

Numerical calculations were performed to quantify the errors due to the uncertainties of the coil position and geometry changes due to the heating in a non-ideal magnetic field. The magnetic field map obtained from an OPERA 2D model was used for this study, assuming no azimuthal field dependence. The magnetic flux density, integrated along the copper wire as a function of the vertical distance between the centre of the coil and the horizontal plane was calculated for the following cases:

1. reference coil position: the coil axis and the air gap axis are perfectly aligned;
2. coil displaced vertically by $10 \mu\text{m}$ relative to the reference coil positions of case 1;
3. coil axis displaced laterally relative to the gap axis by $10 \mu\text{m}$;
4. coil rotated with respect to the horizontal symmetry plane of the magnet by $100 \mu\text{rad}$;
5. coil cross-section increased due to the coil ohmic heating, where 0.4 K is the maximum expected temperature raise of the coil in an hour.

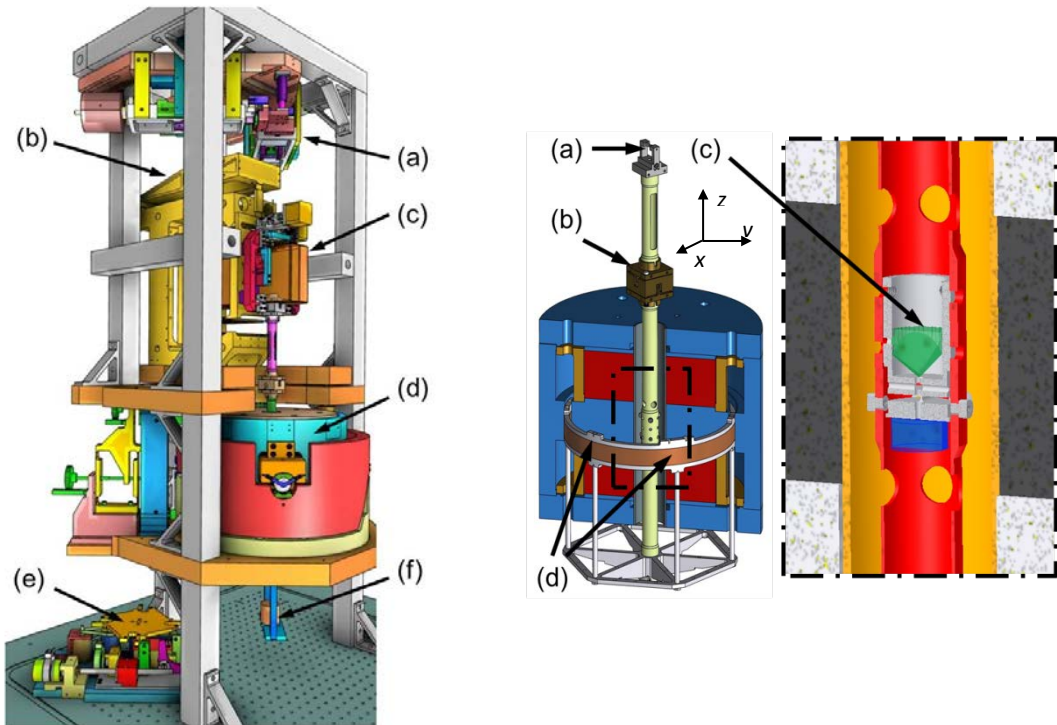


Figure 5. Left: schematic view of the METAS watt balance. The main components are (a) the driving stage, (b) the guiding or translation stage, (c) the mass comparator, (d) the magnetic circuit and its alignment system, and (e) the mass exchanger. The test mass (f) is placed at the bottom of the suspension. Right: The suspension-coil assembly is suspended to the comparator by a double cone hook (a). The upper and lower part of the central tube are linked by a monolithic aluminum flexible double gimbal (b). The determination of the coil position and attitude is done with help of the main central corner cube (c) and the six optical elements (3 flat mirrors, 3 corner cubes) placed on the coil structure (d).

The distribution of the integrated magnetic field BL along the vertical axis for the reference coil position (case 1) is shown in Fig. 6 (left) and the results of the calculations for the cases 2 - 5 in comparison to the case 1 are shown in Fig. 6 (right). It was found that in the ± 10 mm travel range of the coil, the relative change of BL due to the coil lateral displacement, rotation and thermal expansion is less than $\pm 1 \cdot 10^{-8}$. The $\pm 5 \cdot 10^{-7}$ major contribution is due to the vertical displacement of the coil that is directly linked to the magnetic field uniformity along the vertical axis.

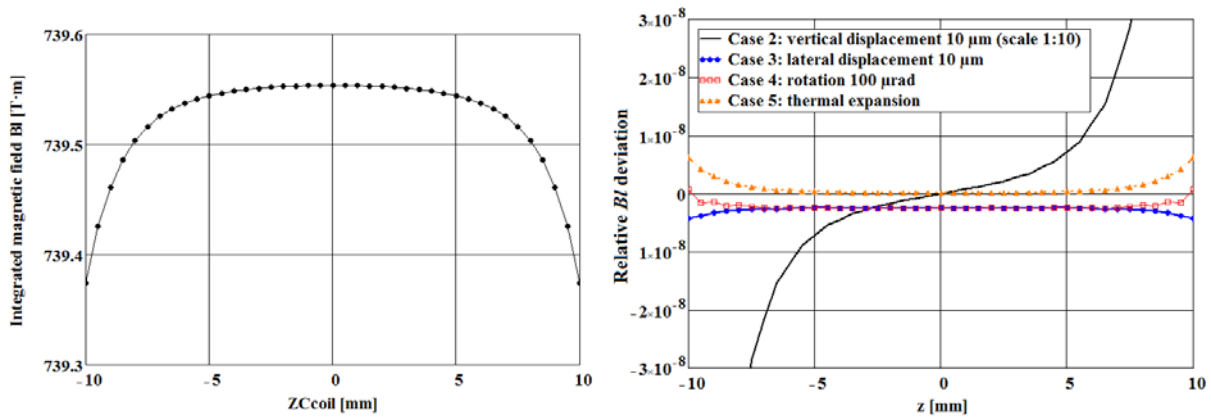


Figure 6. Left: Integrated magnetic field BL vs the vertical position of the coil for the case 1. Right: relative integrated magnetic field deviation (with respect to the case 1) as a function of the vertical position of the coil for the cases 2-5.

The figure 7 shows the coil attitude (left: rotation about the x axis; right: rotation about the y axis) when the coil moves. The coil rotates by about $20 \mu\text{rad}$ about the x axis (from $-10 \mu\text{rad}$ to $10 \mu\text{rad}$) and by about $10 \mu\text{rad}$ about the y axis (from $-5 \mu\text{rad}$ to $5 \mu\text{rad}$). These rotations are significantly smaller than the required limit of some tens of μrad .

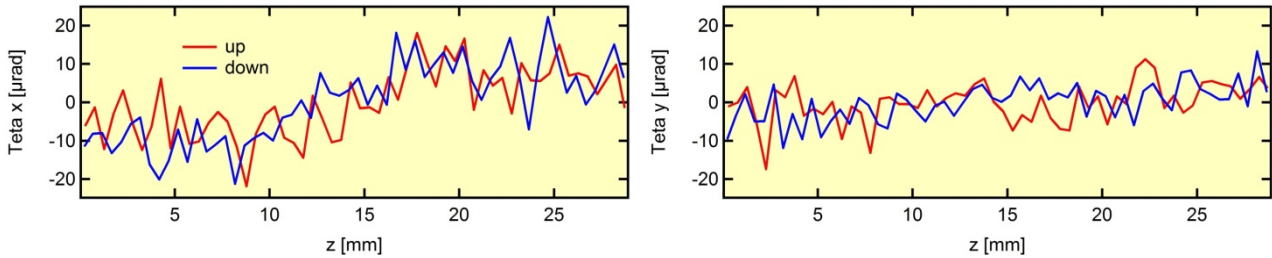


Figure 7. Coil rotations along the trajectory. Left: rotation about the x axis. Right: rotation about the y axis.

The magnetic field is generated by two SmCoGd permanent magnets placed in a closed magnetic circuit. The temperature dependence of the magnetic circuit is drastically reduced by the physical properties of the used magnets and by the 'magnetic shunt', made of a Fe-Ni alloy. With this configuration, a magnetic flux density of 0.65 T with a vertical homogeneity in the order of 10^{-5} and a temperature coefficient better than -5 ppm/K is expected. A preliminary test of the quality of the magnetic field was performed by induction measurements, which correspond to operate the balance in dynamic mode. In this phase the ratio between the induced voltage and the velocity is calculated. This ratio, called the geometrical factor G , gives information about the magnetic field and the mechanical behavior of the coil. During these tests the coil was moved at a velocity of 1.3 mm/s to generate a voltage of about 1 V.

To measure the velocity of the coil, an interferometer developed in-house is used. The working is shown in Fig. 8. Firstly, the incoming beam passes through a half wave ($\lambda/2$) plate to equilibrate the two interferometer arms. Next, it is split by a polarizing splitter (BS1) to originate two interfering beams. The first goes straight to the photo detector (PD). The second goes through the quarter wave plate ($\lambda/4$) down to the moving corner cube (MCC). After reflection, the beam travels to the second beam splitter (BS2) where a part is directed to the x-y position detector (PSD). The other part is delivered to the reference corner cube (RCC). Then the beam moves back to the first splitter where it is delivered to the photo detector (PD). With this design, it is possible to measure both the coil position in the x-y plane and along the z axis.

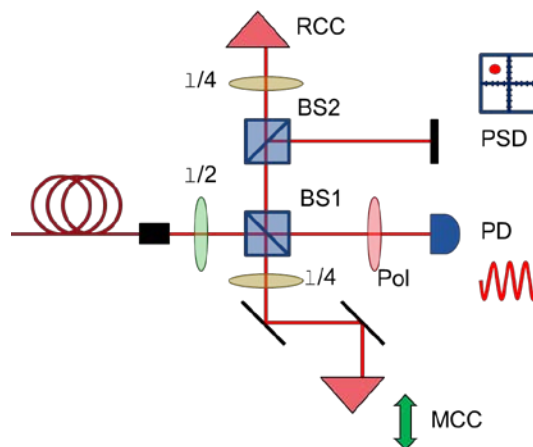


Figure 8. Schematics of the inline interferometer. The incoming laser beam is divided in two. The first beam goes through the splitter (BS1) to the detector (PD). The measuring beam travels from the first splitter to the moving corner cube (MCC). After reflection it moves back to the second splitter (BS2) where one part of the signal is directed to the x-y position detector (PSD) and the other part goes to the reference corner cube (RCC). From the reference corner cube the signal goes back to the first splitter where it is reflected to the photo detector (PD).

The figure 9 shows the geometrical factor $G = U/v$ measured at different points along the vertical path of the coil. The mean value (solid line) is an average of 44 curves taken in 15 minutes. It shows a flat region of almost 15 mm wide with a standard deviation near to 10^{-5} . The residual slope over a region of 5 mm around the weighing position is well below 1 ppm/mm. Even though the velocity regulation and the synchronization of the different instruments are not yet optimized, this curve shows that the homogeneity of the magnetic field satisfies the requirements of the experiment.

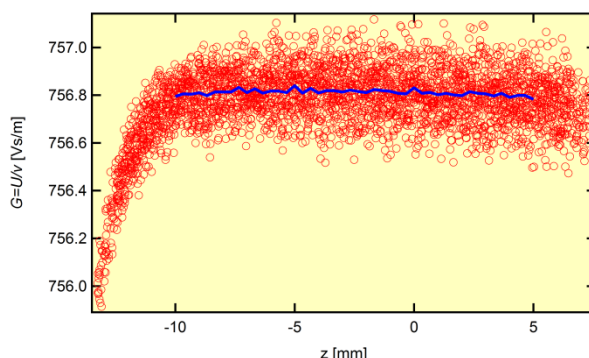


Figure 9. Geometrical factor $G = U/v$ measured in different points along the vertical path of the coil. The solid line is the mean of 44 measurement repetitions. The field profile is flat over a region of almost 15 mm.

The determination of the local value from the gravity acceleration g is measured synchronously with a commercial absolute gravimeter FG5X. Since more than 10 years, the reference station in the METAS watt balance laboratory is measured approximatively once a month. The variation from the gravity over all these years it shown in Fig. 10. The standard deviation of these measurements is $2.6 \mu\text{Gal}$ ($1 \text{ Gal} = 10^{-5} \text{ m/s}^2$).

The reference station is placed beside of the watt-balance experiment. The gravity value measured by the absolute gravimeter must be transferred to the location of the reference mass in the watt balance. Different approaches were proposed for the transfer, where a number of models must be used to estimate the influence of the experimental apparatus itself. In the METAS experiment the transfer will not include any model, but will be based on measurements made inside the experiment apparatus, in a vacuum. This direct tie will be established by a relative gravimeter.

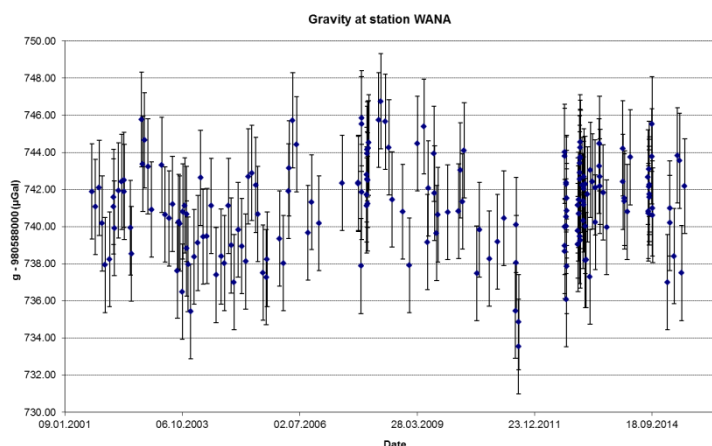


Figure 10. Differences between the gravity values measured on the watt balance and the reference station.

2.5 Measurement of the Avogadro constant

The CIPM and CCM recommended that, before adjusting the values of the fundamental physical constants from which the numerical value of the Planck constant will be adopted, at least three independent experiments, including works from the watt balance and counting atom experiments, must yield consistent values of the Planck constant with relative standard uncertainties not larger than 5×10^{-8} .

The N_A value is obtained from measurements of the molar volume, VM/m , and lattice parameter, a , of a perfect and chemically pure silicon single-crystal. In a formula,

$$N_A = 8MV / (a^3m),$$

where m and V are the crystal mass and volume, M is the mean molar mass, $a^3/8$ is the atom volume, and 8 is the number of atoms in the cubic unit cell. Since the binding energy of the Si atoms is about 5 eV and the mass of a Si atom is about 26 GeV, M and m can be viewed as the molar mass and mass of an ensemble of free atoms. To make the kilogram redefinition possible, the targeted accuracy is $2 \times 10^{-8} N_A$. It follows that the N_A determination requires the measurement of (i) the lattice parameter — by combined x-ray and optical interferometry, (ii) the amount of substance fraction of the Si isotopes and, then, of the molar mass — by absolute mass-spectrometry, and (iii) the mass and volume of two nearly perfect crystal-balls (named AVO28-S5 and AVO28-S8) having about 93 mm diameter.

2.5.1 Molar mass

The molar mass is given in terms of the molar masses and amount of substance fractions of the Si isotopes. The values of the molar mass of the Si isotopes are extremely well known and contributed negligibly to the total uncertainties. The amount-of-substance fractions were measured independently by the PTB, NMIJ, and National Institute of Standards and Technologies, using isotope dilution and multicollector inductively coupled plasma mass spectrometers. In 2011 a discrepancy emerged between the measured values of the molar fractions obtained by the PTB and National Research Council of Canada. A careful analysis of the published data suggested that the usage of NaOH as solvent and matrix diluent, together with possible memory carry-over, contributed to the discrepancy. Therefore, contrary to the 2011 measurements, tetramethylammonium hydroxide was used as solvent and diluent to reduce the baseline level of the ion currents in the mass spectrometry. INRIM measured the amount-of-substance fraction of ^{30}Si by neutron activation using the TRIGA Mark II reactor of the University of Pavia. The INRIM result further supports the amount-of-substance fraction findings of the PTB, NMIJ and NIST (Fig. 11). The data suggest that, at the present level of measurement sensitivity, there are no longitudinal or axial gradients within the enriched crystal. Combining the results, the average molar mass was calculated, with an associated relative standard uncertainty of 5.4×10^{-9} .

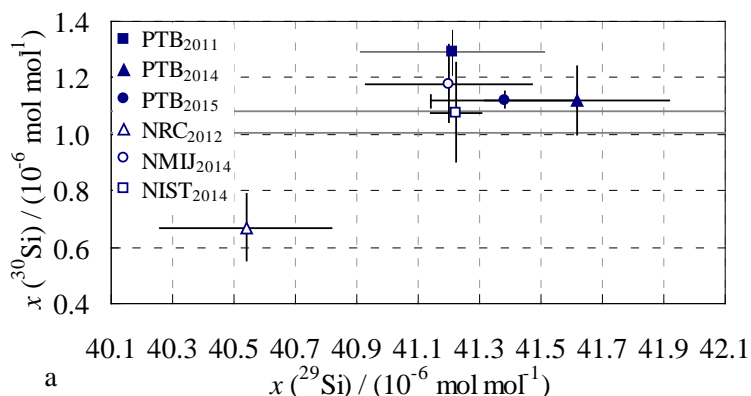


Figure 11. Molar fraction of the minority isotopes in the enriched crystals. The bars indicate the standard errors. The horizontal lines indicate the standard confidence interval of the nuclear activation determination of the ^{30}Si molar fraction.

2.5.2 Lattice parameter

The INRIM's combined x-ray/optical interferometer used to determine the lattice parameter of the enriched crystal was upgraded (Fig. 12). Some weaknesses were pinpointed and eliminated, and measurements repeated to either confirm the 2011 previous result and its uncertainty or to identify errors. In particular, in order to exclude systematic errors in the measurement of the interferometer displacement, the optical interferometer was totally rebuilt and operated at a different wavelength. Diffraction correction was also experimentally assessed, by checking the consistency of measurements carried out with the use of different geometries of the laser beam. A comparison of the INRIM, NMIJ, and PTB temperature measurements was carried out, in order to assess the extrapolation of the atom and crystal volumes – that are measured in different laboratories – to the same temperatures to within uncertainties better than 1 mK. Measurement repetitions confirmed the result of the 2011 one and yielded an additional value having an uncertainty reduced to 1.75 nm/m.

The crystal perfection was investigated by the NMIJ, that carried out topographic measurements of the lattice strain in several crystal samples by means of a self-referenced lattice comparator at the Photon Factory of the High Energy Accelerator Research Organization. The results are consistent with what observed by x-ray interferometry, 1.5 nm/m strains having a typical scale of a few millimeters. A tail-end sample, shows a two dimensional swirl-like pattern and greater strains. This observation is consistent with a contamination-induced strain and the float-zone segregation of impurities into the tail of the crystal.

The IOM investigated plasma etching and ion-beam machining as tools to control the geometrical, physical, and chemical characteristics of the surfaces of the interferometer crystals. The idea was to make it possible to investigate if residual surface stresses (due to dangling bonds, lattice reconstruction, and mismatch between the Si and SiO₂ lattice parameters) affects the lattice parameter measurement. Although ion-beam machining proved capable to shape optimally the interferometer surface, also correcting the geometrical errors caused by wet etching, unavoidable sputtering of contaminants (mainly carbon) caused a so large surface stress to prevent the interferometer operation. Although this problem has not been yet solved, it further strengthens the potential risks that the surfaces can alter the lattice parameter of the interferometer with respect its value in the silicon spheres.

A parallel study of surface effects was started by using a variable thickness interferometer, where the lattice parameter can be sequentially mapped in thick (1.5 mm) and thin (0.5 mm) crystal part. This interferometer was jointly designed and realized by the INRIM and PTB. Although different lattice-parameter values were observed in the thin and thick parts, up to now, the operation of this interferometer gave unexplained results. In particular, large lattice stains were observed that varied after subsequent wet-etching of the crystals. Although we suspect, but cannot yet prove, the presence of a crystal damage caused by the mechanical grinding of so thin crystals, this preliminary tests pointed to a possible surface effect on the lattice parameter value.

The surface can affect the N_A measurement in two ways. The surface strain may sink or raise the ball surface and make the measured volume smaller or greater than the volume of the unstrained ball. The University of Cagliari carried out density functional calculations of the volume difference with atomistic resolution. Surface reconstruction and the presence of an amorphous layer were considered. In the worst case, the sphere volume is smaller than the perfect-crystal volume by about $2.5 \times 10^{-9} V$. The difference is an order of magnitude smaller than the present measurement uncertainty, about $2.0 \times 10^{-8} V$. Secondly, the surface stress may make the lattice parameter of a Si ball different from the value measured in the crystals of an x-ray interferometer, which are only 1 mm thick. First principles investigations are under way and preliminary results indicate that effects on the measured value of the lattice parameter might be observed.

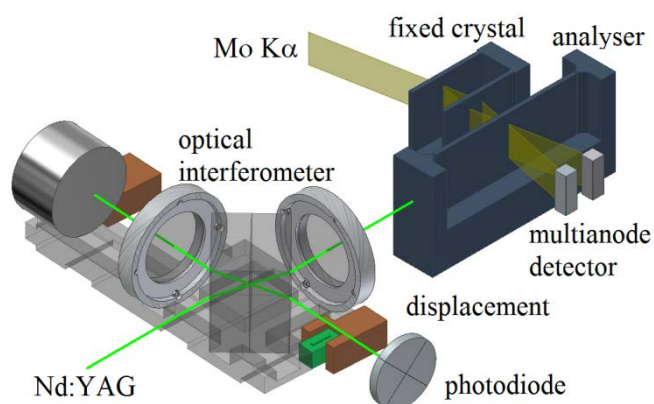


Figure 12. Schematics of the combined x-ray and optical interferometer used to measure the lattice parameter of the enriched silicon crystal.

In order to carry out an independent test of the measured lattice-parameter value and of the systematic effects affecting the measurement, the PTB started the development of an independent measurement apparatus based on significantly different geometries of both the x-ray and optical interferometers. A new concept for the long-distance translation of the interferometer crystal was deeply investigated, but eventually proved to be just as impractical. This work delayed the integration and operation of the full apparatus and prevented measurements to be carried out by the end of the project.

2.5.3 Sphere manufacturing and surface characterization

One of the issues with the 2011 NA determination was the fact that the surface of the ^{28}Si spheres were contaminated by nickel, copper, and zinc. This contamination was characterized as localized in metal silicide islands floating on the silicon matrix. It was later removed by a Freckle etch, which has a selectively high etching rate for silicides. Since the etching degraded the shape of the spheres, they were repolished by PTB, using a new procedure to improve their roundness (Fig. 13). The surface layer was therefore rebuilt and, more importantly, the metallic contaminants were removed. The surface of the repolished sphere was checked by x-ray fluorescence spectrometry, which revealed negligible amounts of foreign metals. Moreover, no subsurface crystal damage was detected when the sphere surfaces were compared with strain free etched reference crystal surfaces by high-resolution x-ray diffractometry. The surface roughness was below 0.2 nm. The sphere topographies were surveyed interferometrically, establishing that the shape of the sphere was defined only by the orientation of the crystallographic axes. Maximum peak-to-valley deviations of the diameter were below 70 nm, in the worst case.

Roundness errors are suspected to be a limiting factor of the accuracy of the volume measurement. Therefore, the IOM investigated ion-beam machining as a tool to better figure the sphere surface. After the re-polishing of a test natural Si-sphere by the PTB, a complete ion-beam figuring was performed. On the most part of the surface the roundness error was reduced below 15 nm peak-to-valley (Fig. 15). The exceptions are the Polar Regions: an accidental contamination occurred at the northern pole and over-etching at the southern pole. The contamination was traced back to a sub-optimum design of the ion beam source and was eliminated. The cause of the over-etching is still under investigation. The processing chain and the used set of parameters proved to be appropriate to reduce the roundness error (peak-to-valley) to below 20 nm. The surface topography after the machining of the complete sphere exhibited a minor deterioration at the stop point. Furthermore a non-linear dependency of etch rate from the etched depth was observed. This might be either due to the influence of the natural silicon oxide layer or to a dependence of the etch rate on the crystal orientation. Furthermore, the surface alteration during ion beam machining – where energetic particles interacts with the surface – has not yet been sufficiently investigated. Without the understanding of these problems the ion-beam machining of ^{28}Si spheres would be too risky and rather pointless. Therefore, IOM and PTB agreed to postpone the targeted figuring of the ^{28}Si sphere and to perform additional test runs in order to fine tune the procedure.

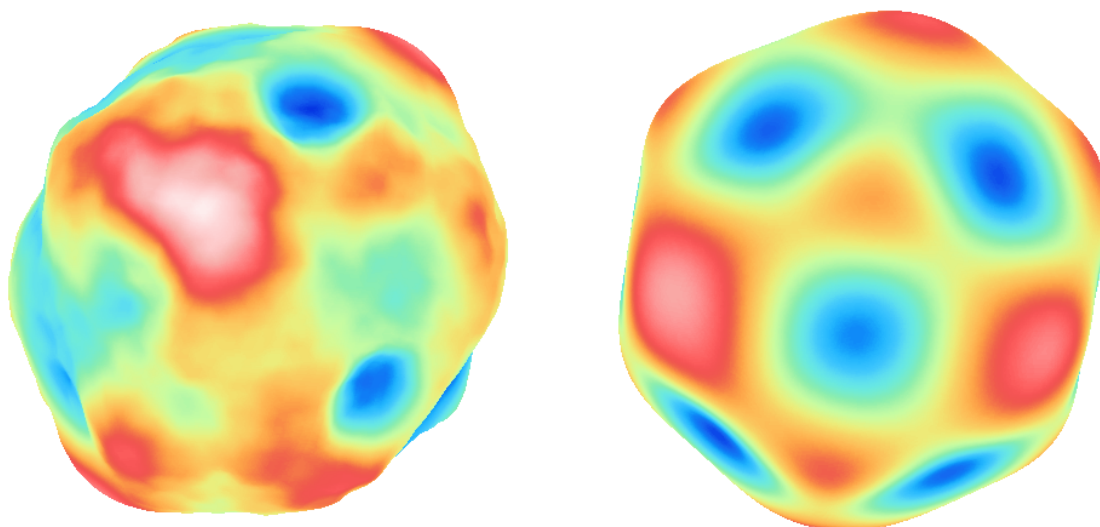


Figure 13. Topography of the sphere surface before (left) and after (right) repolishing.

The measurements of the thickness of the SiO₂ layer were performed at NMIJ and PTB, by using spectral ellipsometers equipped with sphere holders having automatic rotation capabilities. This allowed the surface to be fully covered by a few thousands of measurement points. Spectral ellipsometry has two shortcomings: its accuracy (approximately 1 nm) is insufficient for this application and, as an inverse method, a model of the surface layers is necessary, which becomes part of the measurement process. To overcome these limitations, a calibration must be carried out. This was done by means of references (certified by x-ray reflectometry) at the NMIJ and a combination of x-ray reflectometry and x-ray fluorescence analysis in specific reference-points of the sphere surface by the PTB.

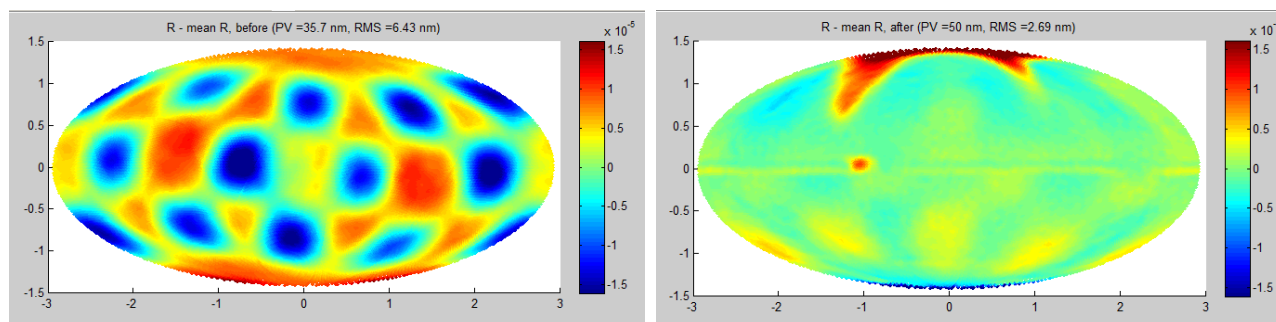


Figure 15. Diameter topography of the surface of a test sphere before (left) and after (right) ion-beam figuring. The same color scale, ranging from -15 nm to +15 nm, has been used.

2.5.4 Sphere volume

The volume of the Si sphere is calculated in terms of the mean diameter $D = D_0 + 2(\Delta R - t_{SL})$, where D_0 is the mean optical diameter, the ΔR correction takes the phase shift of the laser-beam reflection into account, $D_0 + 2\Delta R$ is the mechanical diameter, and t_{SL} is the thickness of the surface layers.

Optical interferometers were used by the NMIJ and PTB to measure the diameters. The measurement takes advantage of a differential approach: first, it measured the spacing of an optical cavity; second, the sphere is placed into the cavity and the gaps are measured. Diameters, measured in many different directions, are obtained by difference.

NMIJ measured a thousand of diameters using an improved optical interferometer with flat etalons. The spheres were placed between the two etalon, and the etalon distance and gaps to the sphere were measured by phase shifting interferometry with optical frequency tuning. The PTB interferometer was based on spherical etalons, so that the etalon forms opposing caps which surround the sphere. The illuminating light was converted by a set of objectives into a focused beam, so that the rays hit the reference etalon-faces and the sphere perpendicularly. Thus, diameters are measured for all points within the field of view (about 60°). This enabled the acquisition of high resolution topographies of the sphere. The excellent agreement between the NMIJ and PTB measurement results gives confidence to the 1.6×10^{-8} final relative uncertainty of the averaged values.

Due to the smaller roundness errors for the repolished spheres, the influence of the wave front aberrations were also presumably reduced, but they remain the principal uncertainty contribution. For this reason the PTB realized a second interferometer, with a set of objectives having considerably reduced wave front aberrations. However, problem pinpointing and solving delayed its operation, a competitive measurement accuracy was achieved only at the project end and investigations of the effect of wave front distortions will be the subject matter of future work.

2.5.5 Sphere mass

The sphere masses were determined by the BIPM, NMIJ, and PTB via comparisons against Pt-Ir or stainless-steel standards both in air and in vacuo. In 2014, the BIPM carried out a calibration campaign with respect to the international prototype, in anticipation of the planned redefinition of the kilogram. This campaign brought to light the existence of an offset in the BIPM as-maintained mass unit, which was traceable to the international prototype in 1992. The corrections applied depend on the date of the BIPM calibrations used for traceability. In the case of NMIJ, the correction was $-30.1(3.0) \mu\text{g}$; in the case of PTB, it was $-35.4(3.0) \mu\text{g}$.

To obtain the total mass of the Si atoms, the sphere mass was corrected by subtracting the mass of the surface layers. The SiO_2 mass was determined as density $- 2.2(1) \text{ g/cm}^3$ – times volume; the $0.028(8) \mu\text{g/cm}^2$ sorption coefficient of the chemisorbed water was used to estimate the mass of the chemisorbed water. The mass of the carbonaceous contaminations was determined by comparing the ratio of the C-K peak to Si-L one against a reference carbon layer and the $\text{CH}_{1.5}$ stoichiometry was assumed. The metallic contamination affecting the 2011 measurements has been removed; therefore, no additional correction was necessary.

The mass of the point-defect was taken into account by correcting the mass values to obtain the mass of a crystal having Si atoms at all lattice sites and no interstitial atoms. The mass deficits were calculated on the basis of the contaminant and vacancy concentrations. The concentrations of dissolved carbon, oxygen, nitrogen, and boron were determined by the PTB via infrared absorption measurements. Contamination data are required to endorse the crystal purity. In particular, it is essential to verify that the total impurity mass-fraction is below a few parts in 10^9 , or to quantify it with an uncertainty smaller than this limit. There is a consensus that the contaminations by the most of the elements are significantly smaller than parts per billion of a Si atom. However, the experimental data are necessary to decrease the risk of biased results or of under-evaluated uncertainties. INRIM developed an elemental analysis method based on nuclear activation giving direct impurity evidence. Measurements carried out at the TRIGA Mark II reactor at the University of Pavia and the OPAL reactor of the Australian Nuclear Science and Technology Organisation included fifty-nine elements and excluded contaminations higher than 1 ng/g for thirty-five elements.

2.5.6 Determination of the Avogadro constant

Table 2 (left) gives the uncertainties of the measurements of the molar mass, lattice parameter, volume, and mass of the enriched silicon spheres. The quantities dominating the total uncertainty of the Avogadro constant were the diameter of the spheres and the mass of the surface layer. The N_A determinations are given in table 2 (right); they differ only by $13(20) \times 10^{-9} N_A$. Averaging these two values, the final value of the Avogadro constant is

$$N_A = 6.022\,140\,76(12) \times 10^{23} \text{ mol}^{-1}$$

with a standard uncertainty of $20 \times 10^{-9} N_A$.

Table 2. Left: uncertainty of the N_A determination (AVO28-S5 sphere). The percent contributions to the total uncertainty are the relevant variance fractions ratio to the total variance. Right: Value of the Avogadro constant based upon the enriched SI spheres.

Quantity	$u_r/10^{-9}$	%
Molar mass	5	6
Lattice parameter	5	6
Surface characterization	10	23
Sphere volume	16	59
Sphere mass	4	4
Point defects	3	2
Total	21	100

Sphere	$N_A/10^{23} \text{ mol}^{-1}$	$u_r/10^{-9}$
AVO28-S5	6.022 140 72(13)	21
AVO28-S8	6.022 140 80(14)	23
Mean value	6.022 140 76(12)	20

2.6 Solving the discrepancies

2.6.1 Speed of light effect in free-fall gravimeters

The local acceleration due to gravity, g , plays a crucial role in the watt balance experiments. The most widely used technique for precision measurements of g is to track the position of a free-falling body by means of a Michelson interferometer. The relative uncertainty of this kind of instrument is nowadays a few parts in 10^9 . This uncertainty is smaller than the perturbation coming from the finite speed of propagation of light in the interferometer. Thus, to properly measure g , the speed of light correction should be taken into account and was calculated by several authors. The given results were recently questioned and a reconsideration of the theoretical derivation was proposed that delivered a different correction. The controversy was deepened by the claim of a correction measurement that apparently confirmed the new proposed value; but, a series of works questioned both the theoretical derivation and experimental result. This controversy has a direct impact on the watt balance experiments; therefore, it called for an independent theoretical analysis and experimental study. The METAS established both theoretically and experimentally the value of the proportionality factor a_c in corrections formula $a_c(gv_0 + g^2 t)/c$, where v_0 is the initial velocity and c is the speed of light. For the experimental determination of a_c , 28 datasets were analysed, which correspond to more than 50'000 drops, from 3 different instruments on 9 different sites. The theoretical result is $a_c = 3$, while the experimental estimate is $a_c = 3.2 \pm 0.2$, to within a 95% confidence interval. This result confirms the usual theoretical treatment of one of the most important corrections necessary to achieve the required relative uncertainty of a few parts in 10^9 in the g measurement.

2.6.2 Coil-magnet interaction: continuous model

The standard description of the watt-balance operation rests on lumped parameter models of the coil-field interaction, where the coil is considered to be one-dimensional. In weighing mode, the magnetic force acting on a three dimensional coil is given by the integral of the density of the Lorentz force over the coil volume. After modelling the coil turns as toroids, the current follows a $1/r$ law and the total force was proved calculable by a one-dimensional coil model. In the moving mode, the voltage between the coil ends can be identified with the electromotive force induced by the motion only if there exists a charge distribution originating an electric field nullifying the Lorentz field, but, in general, there is no electric field preventing eddy currents from flowing in the coil. The one-dimensional model was proved valid when a toroidal coil is coaxially placed in a radial

magnetic field and moved along the field axis. Furthermore, it was also proved valid when a number of aberrations of the coil–field interaction are considered one at a time, with the single case of a coil motion that is not parallel to the field axis remaining undecided.

2.6.3 Coil-magnet interaction: electrostatic forces

The watt balance operation requires that no external force acts on the coil, apart from that due to the interaction between the electric current and the magnetic field. However, stray capacitances exist between the coil and the magnet and the electric current creates a difference in electric potentials between the coil and magnet. These forces were assumed to be irrelevant. The INRIM proved that a finite element analysis has adequate accuracy for investigating their effect and, by using the METAS watt-balance as test-bed, demonstrated the no-effect assumption was indeed correct. Stray capacitances affect also the moving-mode operation: charge and discharge currents induced by the capacitance variations influence the voltage measured between the coils ends. Furthermore, the electrostatic forces acting on the moving coil can induce unwanted velocity components. These effects should be negligible, but they deserve future investigations.

2.6.4 Stress and strain of Si surface

The measurement of N_A is based on the assumption that the Si spheres have a perfect crystal structure up to the outermost atom layers. This is not the case because of the surface relaxation and reconstruction, the possible presence of an amorphous layer, and the oxidation. When the crystal forms a surface, surface relaxation and reconstructions take place. The reconstructions are due to the presence of dangling bonds which tend to rebind forming a network other than the bulk-like one. Relaxations and reconstruction stress and strain the atom layers nearest to the surface. Such surface stress and strain may in turn have a twofold effect on the N_A measurement. Firstly, the surface stress may make the lattice parameter of a Si ball different from the value measured in the crystals of an x-ray interferometer, which are only about 1 mm thick. Secondly, the surface strain may sink or raise the ball surface and make the measured volume smaller or greater than the volume of the unstrained crystal. The Cagliari University carried out density functional theory calculations of surface strain by using the Quantum Espresso computer package with atomistic resolution and aimed at excluding or quantifying systematic surface contributions to the measured N_A value. The results indicate that the surface induced strain, in the worst case, change the volume of the ^{28}Si balls used to determine the Avogadro constant is smaller than the perfect-crystal volume by about $2.5 \times 10^{-9} V$. The difference is an order of magnitude smaller than the present measurement uncertainty, about $2.0 \times 10^{-8} V$, but it is not as small as might be expected and it may be worth considering more accurate measurements in future. First principles calculations of the stress originated by a 1 nm thick (amorphous) SiO_2 layer on the (110) surface of the interferometer crystals are under way. Preliminary results indicate that effects on the measured value of the lattice parameter might be observed.

2.6.5 Nuclear activation determination of the ^{30}Si fraction

The isotope mole-fractions of the Avogadro ^{28}Si -enriched crystal AVO28 has been measured by isotope dilution mass spectroscopy by the Physikalisch-Technische Bundesanstalt (PTB), the National Research Council of Canada (NRC), the National Metrology Institute of Japan (NMIJ), and the National Institute of Standards and Technology (NIST). There is a general agreement among the measurement results, but the NRC differ significantly. Aiming at collecting experimental data with a different technique and at investigating the discrepancy, the INRIM measured ^{30}Si fraction by instrumental neutron activation analysis. The amount of ^{30}Si isotope was determined by counting the 1266.1 keV γ -photons emitted during the radioactive decay of the radioisotope ^{31}Si produced via the neutron capture reaction $^{30}\text{Si}(n,\gamma)^{31}\text{Si}$. The result is consistent with the PTB and NIST values. This agreement rules out a contamination of the isotopic composition results used to calculate the molar mass of the AVO28 material.

2.6.6 Elemental analysis of the ^{28}Si purity by nuclear activation

The crystal used to determine N_A must have a total impurity mass fraction smaller than a few parts in 10^9 . Since the molar mass, lattice parameter and volume are those of each sphere, the sphere masses were corrected for the impurity atoms and vacancies. In this way, we calculated the mass of equivalent spheres, having the same volume and lattice parameter as the real ones, but having a Si atom at each lattice site. The contaminations of carbon, oxygen, boron, and nitrogen were determined by infrared spectroscopy. To verify the 1 ng/g requirement for the largest possible number of contaminants, the project developed a relative analytical method based on neutron activation. The method was applied to a crystal sample of the ^{28}Si crystal. Measurements were carried out at the Laboratorio Energia Nucleare Applicata of the Pavia University and the Australian

Nuclear Science and Technology Organisation. Thirteen contaminants were identified, whose concentrations are between 20 fg/g and 1 ng/g. For other elements detection limits were established: ten are between 1 µg/g and 10 ng/g (about 50 elements) and between 1 ng/g and 10 fg/g (about 40 elements). Future activity will focus on the detection of voids via copper or iridium decoration and the subsequent quantification by nuclear activation.

2.6.7 Consistency of the Planck constant values

Statistical parametric models were used to explain the values of the Planck constant obtained by the watt balance experiments and by counting atoms in ²⁸Si enriched crystals. They assume that uncertainty contributions – having heterogeneous, datum-specific, variances – might not be included in the error budgets of some of the measured values. Model selection and model averaging were used to study data consistency, to identify a reference value of the Planck constant, and to include the model uncertainty in the error budget. The data consistency was studied by explaining the measurement results by random effect – which allow, but do not assume, missing contributions to the error budgets – and fixed effect – which allow, but do not assume, different means of the sampling distributions – models. In both cases, the data look inconsistent. In the first case, after averaging over all the subsets of good data, the mean value is

$$h = 6.626\,070\,073(94) \times 10^{-34} \text{ Js}$$

The standard deviation, $1.4 \times 10^{-8} h$, can be compared with the weighed-mean uncertainty, $1.3 \times 10^{-8} h$. The quadratic difference, $0.5 \times 10^{-8} h$, is the contribution to the error budget of the uncertainty about the actual subset of good data.

2.6.8 Correlation of the N_A measurements

In order to make the N_A values given in 2011 and 2015 usable for a least squares adjustment, their correlation was carefully estimated. The result is summarized in Table 3. Despite these values being obtained by counting twice the atoms in the same ²⁸Si enriched spheres, owing to the sphere-surface repolishing and the upgrades of many of the measurement technologies, their correlation is only 17%. Taking the correlation into account, the average of the 2011 and 2015 values is

$$N_A = 6.022\,140\,82(11) \times 10^{23} \text{ mol}^{-1},$$

with an uncertainty of $1.8 \times 10^{-8} N_A$. To assess the consistency of the N_A values, we observe that their difference is $38(33) \times 10^{-9} N_A$, where we took the 17% correlation into account in the uncertainty calculation.

Table 3. Uncertainty budgets — expressed in parts per 10^9 — of the 2011 and 2015 N_A determinations.

Quantity	2011	2015	correlation
Molar mass	7.9	5.4	0.00
Unit cell volume	10.5	5.5	0.15
Sphere volume	30.2	16.0	0.14
Sphere mass	15.0	11.0	0.32
Total	36.2	20.9	0.17

2.7 Key results

In summary, the key results of the research undertaken are

- an independent watt-balance measurement of the Planck constant;
- an improved molar-mass measurement of the enriched crystal and the elimination of the discrepancy between the NRC and PTB results;
- the strain- and contamination-free polishing of Si spheres to within diameter errors less than 70 nm (AVO28-S5) and 40 nm (AVO28-S8);
- an additional, more accurate, value of the Avogadro constant;

- the solution of the discrepancy between the results of the watt-balance (NIST) and atom counting experiments;
- the complying with the accuracy of the N_A determination required to make the kilogram redefinition possible.

The figure 16 compares the most recent results of the watt-balances and atom counting experiments, expressed in terms of the Planck constant value.

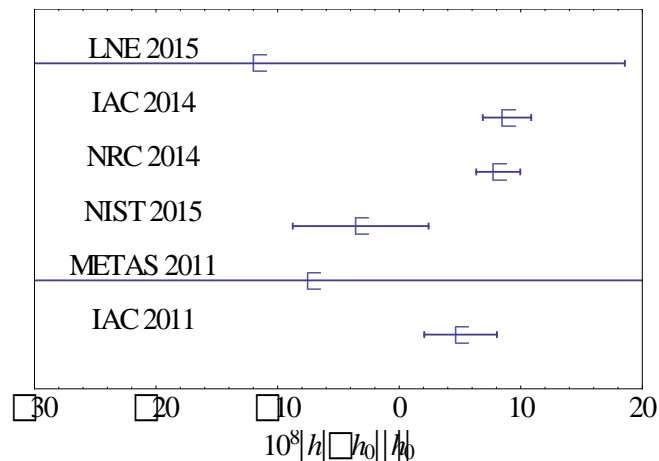


Figure 16. Results of the most recent determinations of the Planck constant. The IAC 2014 and LNE 2015 labels indicate the values delivered by this project. h_0 is the value internationally recommended by the CODATA in 2010.

3 Actual and potential impact

By contributing to strengthen the foundation of metrology, the project impact was mainly on measurement science and technology. The development of the technologies necessary to put the kilogram redefinition in practice is a big step towards a redefinition of the whole system of measurement units, which is expected to deliver even more solid foundations and reliability to precision measurements and to set the stage for further innovations in technology and science.

Following the CGPM resolution on the future revision of the international system of units, on November 2014, the CIPM set out a detailed roadmap towards the change. The CIPM and CCM recommended that following conditions are met before adjusting the values of the fundamental physical constants from which the numerical value of the Planck constant will be adopted:

1. At least three independent experiments, including works from the watt balance and counting atom experiments, must yield consistent values of the Planck constant with relative standard uncertainties not larger than 5×10^{-8} ,
2. At least one of these results should have a relative standard uncertainty not larger than 2×10^{-8} ,
3. The BIPM prototypes, the BIPM ensemble of reference mass standards, and the mass standards used in the watt balance and counting atom experiments must be compared as directly as possible with the international prototype of the kilogram,
4. The procedures for the future realization and dissemination of the kilogram, as described in the mise en pratique, must be validated in accordance with the principles of the CIPM-MRA.

The joint CCM and CCU roadmap towards the redefinition of the SI in 2018 plans for the meeting of the recommendation 3 by the middle of 2015 and of the recommendations 1 and 2 by the middle of 2016.

The main motivation of the project was to remove – jointly with parallel works carried out by the NIST and NRC – the discrepancies observed between the 2010 results of the watt-balance and atom count experiments. The two completely different experiments achieved now results that both are precise enough, and in sufficient agreement, to topple the present definition. Also based on the project results, in August 2015, the CODATA task group on fundamental constants recommended a value of the Planck's constant having a $12 \times 10^{-9}h$

uncertainty, over one-quarter of the uncertainty previous reported and within the requirements to make the kilogram redefinition possible.

The project's determination of the Avogadro and Planck constants via atom counting, fulfilled the directions of the recommendations 1 and 2 and contributed via the participation and the information delivered to the CCM and the relevant consultative committees, to the drafting of the *mise en pratique* – a set of instructions that allows the definition to be realized in practice at the highest level. The LNE and METAS, although they did not yet deliver values of the Planck constant fulfilling the recommendations, progressed the European independence in this approach to the kilogram realization. Besides, to date, only the watt balance experiment run by the NRC (Canada) complies with CIPM recommendations, but many competing experiments have been put on the track worldwide.

The project demonstrated a successful *mise en pratique* of a kilogram definition based upon a fixed value of the Planck constant. Because effects of crystal imperfections have not yet been detected, the count uncertainty is still limited by the performance of the measurement apparatuses. Therefore, provided the source material is chemically and physically well characterized with respect to i) the mass fractions of the minor isotopes and impurities, ii) the value of the lattice parameter, and the iii) crystallographic perfection, material realizations of the kilogram and its submultiples in the form of crystal spheres require only volume measurements and surface characterizations. These same two parameters would also be the only two quantities necessary to monitor the secular stability of the artefacts.

Once the invariant sphere-properties – that is, crystallographic perfection, chemical and isotopic purity, and lattice parameter – have been quantified, the count reduces to the measurement of the variable quantities – that is, geometrical, physical, and chemical characterization of the surface and volume. In practice, this corresponds to label a sphere by its density – instead of its mass – and, following Newton, to obtain its mass via volume measurements and surface characterization.

Long term impact is conditioned by the cost of enriched silicon that prevents the laboratories that did not participate to the IAC to have kilogram realizations by ^{28}Si spheres. However, to realize a sphere that does not require recalibration by mass measurements, accepting that it is calibrated for the first time by a mass comparison against a ^{28}Si standard, the use of enriched silicon is not strictly necessary. In fact, only the variable part of the atom-count procedure needs to be repeated and this recount does not depend on how the count was done the first time. Therefore, relatively cheap spheres – in principle, having the same crystallographic, chemical, and geometric perfections as a ^{28}Si sphere – can be manufactured by using natural silicon. In principle, these standards will never require mass comparisons to be recalibrated and, if a breakthrough will make an accurate determination of the isotopic composition possible, they open the door to a future spread of primary realizations.

In the long term, natural silicon spheres will be a tool to make kilogram realizations accessible to any laboratory capable to carry out surface characterizations and volume measurements. In addition, being improved material standards, silicon spheres will affect minimally the kilogram dissemination. Verifications will no longer be constrained by fears of irreversible mass changes, because mass changes can be also identified, quantified, and explained by the parallel observation of volume and surface changes. Eventually, contrary to Pt-Ir standards, there are not (or significantly smaller) cost barriers to the usage of natural silicon mass-standards in secondary laboratories and industries.

The project originated:

- 57 publications in peer reviewed journals;
- 60 communications at conferences;
- 1 master thesis and 3 PhD thesis;
- 23 training events (internships, classes, and workshops for internal and external audience);
- 22 participations and/or communications to metrology committees (CODATA task group on fundamental constants, CIPM committees and working groups, EURAMET technical committee);
- 29 dissemination activities (events, web sites, press releases, articles in trade/professional and popular press interviews, TV clips)

- 8 research collaborations at the European and International level.

4 Website address and contact details

JRP coordinator: Giovanni Mana
INRIM – Istituto Nazionale di Ricerca Metrologica
str delle cacce, 91 10135 Torino Italy
Tel +39 011 3919 728 / 760
e.mail g.mana@inrim.it

JRP website: <http://www.inrim.it/know/>

5 Participants and collaborators

J Bennet, A Stopic

ANSTO – Australian Nuclear Science and Technology Organisation – Australia

Y Azuma, N Kuramoto, K Fujii, H Fujimoto, S Mizushima, A Waseda, L Zhang

AIST-NMIJ – National Measurement Laboratory of Japan – Japan

M Stock

BIPM – Bureau International des Poids et Mesures

D Tommasini

CERN – European Organization for Nuclear Research – Switzerland

P Juncar, P Pinot

CNAM – Conservatoire National des Arts et Métiers – France

R Clavel

EPFL-LSRO – Laboratoire de Systemes Robotique – Switzerland

T Arnold, F Pietag, H Paetzel

IOM – Leibniz Institute of Surface Modification – Germany

G D’Agostino, G Mana, E Massa, C P Sasso

INRIM – Istituto Nazionale di Ricerca Metrologica – Italy

A Allaoua, F Bielsa, Y Briand, C Cayron, P Espel, F Koumondji, J-L Laurent, V Morazzani, M Thomas,

P Tuckey B Franck, F Piquemal

LNE – Laboratoire national de métrologie et d’essais – France

A Eichenberger, H Baumann

METAS – National Metrology Institute – Switzerland

D Reber

Mettler Toledo – Switzerland

S Merlet, F Pereira

OBSPARIS – Observatoire de Paris – France

G Bartl, H Bettin, I Busch, M. Borys, U Kuetgens, K Friedrich, T Mai, A Nicolaus, A Pramann

PTB – Physikalisch Technische Bundesanstalt – Germany

L Colombo, C Melis

UNICA – Cagliari University – Italy

6 List of acronyms

BIPM : Bureau International des Poids et Mesures
 CIPM : International Committee for Weights and Measures
 CCM : Consultative Committee for Mass and Related Quantities
 CCU : Consultative Committee for Units
 CGPM : Conférence Générale des Poids et Mesures
 CODATA : Committee on Data for Science and Technology
 EURAMET : European Association of National Metrology Institutes
 IAC : International Avogadro Coordination
 IPK : International Prototype of the kilogram
 NIST : National Institute of Standards and Technology
 NRC : Measurement Science and Standards Laboratory, Canada's National Research Council
 SI : International system of units

7 List of publications

- Andreas, B, K Fujii, N Kuramoto, and G Mana. "The uncertainty of the phase-correction in sphere-diameter measurements." *Metrologia* 49, no. 4 (2012): 479.
- Andres, B., G. Mana, E. Massa, and C. Palmisano. "Modeling laser interferometers for the measurement of the Avogadro constant." 2014.
- Arnold, Thomas, and Fred Pietag. "Ion beam figuring machine for ultra-precision silicon spheres correction ." *Precision Engineering* 41 (2015): 119-125.
- Azuma, Y, et al. "Improved measurement results for the Avogadro constant using a ²⁸Si-enriched crystal." *Metrologia* 52, no. 2 (n.d.).
- Azuma, Y, et al. "Improved measurement results for the Avogadro constant using a ²⁸Si-enriched crystal." *Metrologia* 52, no. 2 (2015): 360.
- Bartl, Guido, Michael Krystek, and Arnold Nicolaus. "PTB's enhanced stitching approach for the high-accuracy interferometric form error characterization of spheres." *Measurement Science and Technology* 25, no. 6 (2014): 064002.
- Baumann, H., et al. "Design of the new METAS watt balance experiment Mark II." *Metrologia* 50, no. 3 (2013).
- Becker, Peter. "The new kilogram definition based on counting the atoms in a ²⁸Si crystal." *Contemporary Physics* 53, no. 6 (2012): 461-479.
- Bergamaschi, L., G. D Agostino, L. Giordani, G. Mana, and M. Oddone. "The detection of signals hidden in noises." *Metrologia* 50, no. 3 (2013).
- Bettin, H., K. Fujii, J. Man, G. Mana, E. Massa, and A. Picard. "Accurate measurements of the Avogadro and Planck constants by counting silicon atoms." *Annalen der Physik*, 6 2013: 1-8.
- Cosandier, F, et al. "Development and integration of high straightness flexure guiding mechanisms dedicated to the METAS watt balance Mark II." *Metrologia* 51, no. 2 (2014): S88.
- D Agostino, G, G Mana, M Oddone, M Prata, L Bergamaschi, and L Giordani. "Neutron activation analysis of the ³⁰Si content of highly enriched ²⁸Si: proof of concept and estimation of the achievable uncertainty." *Metrologia* 51, no. 3 (2014).
- D'Agostino, G, G Mana, M Oddone, M Prata, L Bergamaschi, and L Giordani. "Neutron activation analysis of the ³⁰ Si content of highly enriched ²⁸ Si: proof of concept and estimation of the achievable uncertainty." *Metrologia* 51, no. 3 (2014): 354.
- D'Agostino, G, L Bergamaschi, L Giordani, G Mana, and M Oddone. "Instrumental neutron activation analysis of an enriched ²⁸Si single-crystal." *Journal of Radioanalytical and Nuclear Chemistry* 299, no. 1 (2013).
- D'Agostino, G, L Bergamaschi, L Giordani, G Mana, and M Oddone. "Instrumental neutron activation analysis of an enriched ²⁸Si single-crystal." *Journal of Radioanalytical and Nuclear Chemistry* 299, no. 1 (2013).
- D'Agostino, G, L Bergamaschi, L Giordani, G Mana, and M Oddone. "Instrumental neutron activation analysis of an enriched ²⁸Si single-crystal." *Journal of Radioanalytical and Nuclear Chemistry* 299, no. 1 (2013).
- D'Agostino, G., L. Bergamaschi, L. Giordani, G. Mana, E. Massa, and M. Oddone. "Elemental characterisation of the Avogadro silicon crystal WASO 04 by neutron activation analysis." *Metrologia* 49, no. 6 (2012).
- D'Agostino, Giancarlo, Marco Di Luzio, Giovanni Mana, Massimo Oddone, Axel Pramann, and Michele Prata. "³⁰Si Mole Fraction of a Silicon Material Highly Enriched in ²⁸Si Determined by Instrumental Neutron Activation Analysis." *Analytical Chemistry* (American Chemical Society) 87, no. 11 (5 2015): 5716-5722.

- Farah, Tristan, Pierre Gillot, Bing Cheng, Arnaud Landragin, S{e}bastien Merlet, and Franck Pereira dos Santos. "Effective velocity distribution in an atom gravimeter: Effect of the convolution with the response of the detection." *Phys Rev A (APS)* 90, no. 2 (8 2014): 023606.
- Farah, Tristan, Pierre Gillot, Bing Cheng, Arnaud Landragin, S{e}bastien Merlet, and Franck Pereira dos Santos. "Effective velocity distribution in an atom gravimeter: Effect of the convolution with the response of the detection." *Phys Rev A (APS)* 90, no. 2 (8 2014): 023606.
- Francis et al., Olivier. "The European Comparison of Absolute Gravimeters 2011 (ECAG-2011) in Walferdange, Luxembourg: results and recommendations." *Metrologia* 50, no. 3 (2013).
- Gillot, Pierre, Olivier Francis, Arnaud Landragin, Franck Pereira dos Santos, and S{e}bastien Merlet. "Stability comparison of two absolute gravimeters at their best capabilities: optical versus atomic interferometers." *Metrologia* (IOP Publishing) 51, no. 5 (6 2014): L15.
- Gillot, Pierre, Olivier Francis, Arnaud Landragin, Franck Pereira dos Santos, and S{e}bastien Merlet. "Stability comparison of two absolute gravimeters at their best capabilities: optical versus atomic interferometers." *Metrologia* (IOP Publishing) 51, no. 5 (6 2014): L15.
- Jiang et al., Z. "On the gravimetric contribution to watt balance experiments." *Metrologia* 50, no. 5 (9 2013).
- Kuramoto, N., Y. Azuma, H. Inaba, Feng-Lei Hong, and K. Fujii. "Improvements to the Volume Measurement of 28Si Spheres to Determine the Avogadro Constant." *Instrumentation and Measurement, IEEE Transactions on* 64, no. 6 (June 2015): 1650-1656.
- Mai, T., Bartl, G., Nicolaus, A., Peter, A.,. "Characterizing the New Sphere Interferometer for the Diameter Determination of the Avogadro Spheres." *Key Engineering Materials* 613 (2014): 11-16.
- Mana, G., and C Palmisano. "Interval estimations in metrology." *Metrologia* 51, no. 3 (2014): 191.
- Mana, G., P. A Giuliano Albo, and S Lago. "Bayesian estimate of the degree of a polynomial given a noisy data sample." *Measurement* 55, no. September 2014 (2014).
- Mana, G., and E. Massa. "The Avogadro and the Planck constants for redefinition of the kilogram." *rivista del nuovo cimento* (Italian Physical Society) 35, no. 7 (2012).
- Mana, G., E. Massa, and M. Predescu. "Model selection in the average of inconsistent data: an analysis of the measured Planck-constant values." *Metrologia* 49, no. 4 (2012).
- Mana, Giovanni, et al. "The correlation of the NA measurements by counting 28Si." *Journal of Physical and Chemical Reference Data* (American Institute of Physics) 44, no. - (2015): 031209.
- Massa, E., and G. Mana. "An automated resistor network to inspect the linearity of resistance-thermometry measurements." *Measurement Science and Technology* 24, no. 10 (2013).
- Massa, Enrico, Carlo Paolo Sasso, Carlo Palmisano, Giovanni Mana, and Carlo Sasso. "A more accurate measurement of the 28Si lattice parameter." *Journal of Physical and Chemical Reference Data* (AIP) 44, no. 3 (2015): 031208.
- Melis, C, L Colombo, and G Mana. "Lattice strain at c-Si surfaces: a density functional theory calculation." *Metrologia* 52, no. 2 (2015): 214-221.
- Merlet, S{e}bastien, et al. "D{e}termination de l'acc{e}l{e}ration de la pesanteur pour la balance du watt du LNE." *Revue Fran{c}aise de M{e}trologie (LNE)* 36, no. 2014-04 (9 2014): 11.
- Merlet, S{e}bastien, et al. "D{e}termination de l'acc{e}l{e}ration de la pesanteur pour la balance du watt du LNE." *Revue Francaise de M{e}trologie (LNE)* 36, no. 2014-04 (9 2014): 11.
- Mizushima, S., N. Kuramoto, K. Ueda, and K. Fujii. "Mass Measurement of 1-kg Silicon Spheres for Determination of the Avogadro and Planck Constants." *Instrumentation and Measurement, IEEE Transactions on* 64, no. 6 (June 2015): 1527-1532.
- Nicolaus, A., Bettin, H., Borys, M., Kuetgens, U., Pramann, A.,. "Revision of the SI: The Determination of the Avogadro Constant as the Base for the Kilogram." *Key Engineering Materials* 613 (2014): 3-10.
- Nicolaus, A., Mee{B}, R., Bartl, G.,. "New Avogadro Spheres for the Redefinition of the Kilogram." *Key Engineering Materials* 613 (2014): 17-25.
- Nicolaus, R., et al. "Current State of Avogadro 28Si sphere S8." *IEEE TRANSACTIONS ON INSTRUMENTATION AND MEASUREMENT* 62, no. 6 (2013): 1499-1505.
- Paetzelt, H, G Bahm, and Th Arnold. "Etching of silicon surfaces using atmospheric plasma jets." *Plasma Sources Science and Technology* 24, no. 2 (2015): 025002.
- Paetzelt, H., T. Arnold, G. Boehm, F. Pietag, and A. Schindler. "Surface Patterning by Local Plasma Jet Sacrificial Oxidation of Silicon." *Plasma Processes and Polymers* 10, no. 5 (2014).
- Pinot, P., and G. Genev{e}s. "Characterization of flexure hinges for the French watt balance experiment." 2013.
- . "Characterization of flexure hinges for the French watt balance experiment." 2013. 5.
- Quagliotti, D, and G. Mana. "Stray capacitances in the watt balance operation: electrostatic forces." *Metrologia* 51, no. 2 (2014).

- Quagliotti, D., G. Mana, E. Massa, C. Sasso, and U. Kuetgens. "A finite element analysis of surface-stress effects on measurement of the Si lattice parameter measurement." *Metrologia* 50, no. 3 (2013).
- Sasso, C P, E Massa, and G Mana. "The watt balance operation: a continuous model of the coil interaction with the magnetic field." *Metrologia* 51, no. 2 (3 2014).
- Sasso, C P, E Massa, and G Mana. "The watt-balance operation: magnetic force and induced electric potential on a conductor in a magnetic field." *Metrologia* 50, no. 2 (2013): 164.
- Sasso, C., E. Massa, and G. Mana. "The watt-balance operation: magnetic force and induced electric potential on a conductor in a magnetic field." *Metrologia* 50, no. 2 (2013).
- Thomas, M, et al. "First determination of the Planck constant using the LNE watt balance." *Metrologia* 52, no. 2 (2015): 433.
- Thomas, Matthieu, et al. "Minimization of the coil movement of the LNE watt balance." *Metrologia* 51 (2014): S54, S64.
- Waseda, A., H. Fujimoto, Xiao Wei Zhang, N. Kuramoto, and K. Fujii. "Homogeneity Characterization of Lattice Spacing of Silicon Single Crystals." *Instrumentation and Measurement, IEEE Transactions on* 64, no. 6 (June 2015): 1692-1695.
- Zhang, Lulu, Y. Azuma, A. Kurokawa, N. Kuramoto, and K. Fujii. "Surface Layer Analysis of Si Sphere by XRF and XPS." *Instrumentation and Measurement, IEEE Transactions on* 64, no. 6 (June 2015): 1509-1513.